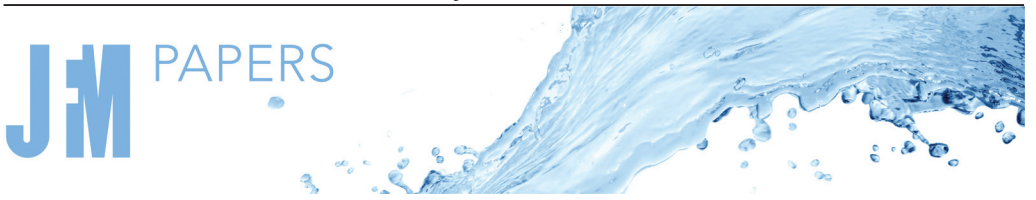
J. Fluid Mech. (2021), *vol*. 929, A31, doi:10.1017/jfm.2021.869



Asymptotic analysis of initial flow around an impulsively started circular cylinder using a Brinkman penalization method

Y. Ueda[1],† **and T. Kida**[2]

[1]Department of Mechanical Engineering, Faculty of Science and Engineering, Setsunan University, 17–8 Ikeda-Nakamachi, Neyagawa, Osaka 572-8508, Japan

[2]Professor Emeritus, Osaka Prefecture University, 1-1 Gakuen-cho, Naka-ku, Sakai, Osaka, 599-8531 Japan

(Received 25 February 2021; revised 1 September 2021; accepted 30 September 2021)

The initial flow past an impulsively started translating circular cylinder is asymptotically analysed using a Brinkman penalization method on the Navier–Stokes equations. The asymptotic solution obtained shows that the tangential and normal slip velocities on the cylinder surface are of the order of $1/\sqrt{\lambda}$ and $1/\lambda$, respectively, within the second approximation of the present asymptotic analysis, where λ is the penalization parameter. This result agrees with the estimation of Carbou & Fabrie (*Adv. Diff. Equ.*, vol. 8, 2003, pp. 1453–1480). Based on the asymptotic solution, the influence of the penalization parameter λ is discussed on the drag coefficient that is calculated using the adopted three formulae. It can then be found that the drag coefficient calculated from the integration of the penalization term exhibits a half-value of the results of Bar-Lev & Yang (*J. Fluid Mech.*, vol. 72, 1975, pp. 625–647) as $\lambda \to \infty$.

Key words: vortex dynamics, computational methods

1. Introduction

Computational fluid dynamics in complicated time-changing geometries is still a major challenging problem and requires advanced numerical techniques. Although various computational fluid dynamics approaches such as a finite volume method have been developed, a vortex particle method is one of highly efficient numerical methods for the simulation of an incompressible viscous flow around a bluff body. The numerical simulation around a bluff body enforces the no-slip boundary condition and also in the vortex method a boundary element method is associated for the no-slip condition (see Koumoutsakos, Leonard & Pépin 1994; Koumoutsakos & Leonard 1995). To overcome the enforcement of the no-slip boundary condition, the Brinkman penalization techniques

† Email address for correspondence: yoshiaki.ueda@mec.setsunan.ac.jp

© The Author(s), 2021. Published by Cambridge University Press

https://doi.org/10.1017/jfm.2021.869 Published online by Cambridge University Press

have been employed together with grid-based numerical methods such as the volume penalization method (see e.g. Schneider & Farge 2002, 2005; Kadoch *et al.* 2012; Schneider *et al.* 2014; Engels *et al.* 2015; Uchiyama *et al.* 2020) and the vortex penalization method (see e.g. Gazzola *et al.* 2011; Rasmussen, Cottet & Walther 2011; Hejlesen *et al.* 2015). In particular, Schneider & Farge (2002) combined the volume penalization method with the wavelet method, and Gazzola *et al.* (2011) applied the vortex penalization method coupled with the grid-based vortex-in-cell (VIC) method to a self-propelled deformable body.

In the latter computation, a level-set function is used to track an interface. Hejlesen *et al.* (2015) shows the validation of the vortex penalization method using an iterative method on the penalization layer to satisfy the no-slip boundary condition. As shown in their studies, the penalization approach is a powerful technique for the simulation of a complicated deformable geometry.

The convergence analysis of the penalization methods for the Navier–Stokes flow is given by Angot, Bruneau & Fabrie (1999) and the error estimation is derived as the order of $1/\lambda^{1/4}$ where λ is the penalization parameter. In this paper, the two-dimensional flow around a square cylinder in a channel is also carried out numerically and the theoretical results are discussed. Further, Angot (2011) proposed a well-posed model for the Stokes flow with jump boundary conditions. Bost, Cottet & Maitre (2010) show the convergence analysis extending the analysis of Angot *et al.* (1999). Also, Feireisl, Neustupa & Stebel (2010) showed the convergence for compressible flows. Kadoch *et al.* (2012) analysed a one-dimensional diffusion equation and the error of the L^2-norm is $O(1/\sqrt{\lambda})$ in a fluid domain and $O(1/\lambda^{1/4})$ in a solid domain. Furthermore, they verified the computed flows around moving circular cylinders. Carbou & Fabrie (2003) analysed the penalization model of the Navier–Stokes equations of a viscous incompressible flow for a small parameter of $\epsilon = 1/\sqrt{\lambda}$ using the Wentzel–Kramers–Brillouin (known as WKB) method, and the error estimation in a fluid domain is shown to be of the order of ϵ, unlike Angot *et al.* (1999). Carbou (2004) studied the porous thin layer model for the interface of a solid boundary on the penalized Navier–Stokes equations and the error is shown to be of the order of ϵ in a fluid domain. Furthermore, he has studied the double penalization model in which one adds the penalization term to the thin porous layer, and showed that the error is also ϵ in a fluid domain (see Carbou 2008). Nguyen van yen, Kolomenskiy & Schneider (2014) analysed the Laplace and Stokes operators with Dirichlet boundary conditions of the volume penalization using a spectral approach and carried out the dipole–wall collision numerically (see Nguyen van yen, Farge & Schneider 2011). In their studies, they derived the Navier boundary condition for the tangential velocity.

In the numerical works of the volume and vortex penalization methods, the initial flow past an impulsively started circular cylinder is selected as a benchmark target (see e.g. Schneider & Farge 2002; Kevlahan & Vasilyen 2005; Kolomenskiy & Schneider 2009; Rossinelli *et al.* 2010; Rasmussen *et al.* 2011; Hejlesen *et al.* 2015; Mimeau, Cottet & Mortazavi 2015; Verma *et al.* 2017). This flow is solved analytically by Bar-Lev & Yang (1975) using the method of matched asymptotic expansions based on the conventional Navier–Stokes equations. Furthermore, Collins & Dennis (1973) studied this flow which is valid for times beyond the first separation, using the power series of time. The initial stage of the circular cylinder impulsively started, rotating and translating from rest is also obtained by Badr & Dennis (1985). Also, Al-Mdallal (2012) and Mittal, Ray & Al-Mdallal (2017) treated the initial stage of a circular cylinder impulsively started with streamwise and transverse oscillations and further rotational oscillation.

https://doi.org/10.1017/jfm.2021.869 Published online by Cambridge University Press

In this study, we analyse the initial flow past an impulsively started translating circular cylinder using the method of matched asymptotic expansions for the Brinkman penalization model of the full Navier–Stokes equations. The previous findings of this flow have been obtained well, so that it can be a good benchmark target. The aim of the present work is to know the explicit characteristic of the Brinkman penalization model, by obtaining the asymptotic solutions of the target flow explicitly. In this study, we compare the present asymptotic solutions with the previous asymptotic solutions of Bar-Lev & Yang (1975) that are obtained from the conventional Navier–Stokes equations. In addition, we estimate the difference of the solution, which arises due to the penalization, against the conventional Navier–Stokes flow.

In § 2, we will briefly present the governing equations of the Brinkman penalization method. In this paper, the relative coordinate systems fixed with the cylinder are taken as the same as in Bar-Lev & Yang (1975), so that the cylinder can be quiescent. The asymptotic solutions are then obtained using the Laplace transform from the governing penalization vorticity equation in § 3. In § 3.6, the drag coefficient will be discussed using three approaches: (1) the integration of the penalization term; (2) the pressure and viscous force on the cylinder surface; and (3) the time derivative of the momentum of the fluid region. In particular, we will compare the present results with the conventional solution of Bar-Lev & Yang (1975) for the case of $\lambda \to \infty$.

2. Governing equations based on the Brinkman penalization

We consider an unsteady incompressible viscous flow that is governed by the Navier–Stokes equations. In the Brinkman penalization model, the governing equation based on the Navier–Stokes equations is written as

$$\frac{\partial \boldsymbol{u}}{\partial t} + \boldsymbol{u} \cdot \boldsymbol{\nabla} \boldsymbol{u} = -\frac{1}{\rho} \boldsymbol{\nabla} p + \nu \nabla^2 \boldsymbol{u} + \lambda \chi (\boldsymbol{u}_S - \boldsymbol{u}), \tag{2.1}$$

where $\boldsymbol{u}$ is the velocity which fulfils the divergence-free condition of $\boldsymbol{\nabla} \cdot \boldsymbol{u} = 0$, p is the pressure, ρ is the fluid density which is assumed to be constant and ν is the kinematic viscosity. Also, $\boldsymbol{u}_S$ denotes the velocity of a solid body. In the present paper the relative coordinate system fixed with the centre of a body is employed and, therefore, the body does not move, i.e. $\boldsymbol{u}_S = 0$. The third term on the right-hand side of (2.1) accounts for the penalization term to impose the no-slip boundary condition. The characteristic function χ defines the domain of active penalization, i.e.

$$\chi = \begin{cases} 1, & \boldsymbol{x} \in \bar{\mathcal{S}}, \\ 0, & \boldsymbol{x} \in \mathcal{F}, \end{cases} \tag{2.2}$$

in which $\mathcal{S}$ denotes the domain occupied by the solid body and $\mathcal{F}$ is the domain occupied by the fluid. In addition, λ is the penalization parameter. The conventional Navier–Stokes equations are found to be recovered in the fluid domain. The penalization approach regards a solid body as a porous media with the permeability being vanishingly small. This results in the fluid velocity being zero at a solid–fluid interface so that the penalization parameter can be required to be sufficiently large.

Taking the curl of (2.1), we can obtain the two-dimensional vorticity equation

$$\frac{\partial \boldsymbol{\omega}}{\partial t} + \boldsymbol{u} \cdot \boldsymbol{\nabla} \boldsymbol{\omega} = \nu \nabla^2 \boldsymbol{\omega} + \lambda \boldsymbol{\nabla} \times [\chi (\boldsymbol{u}_S - \boldsymbol{u})], \tag{2.3}$$

https://doi.org/10.1017/jfm.2021.869 Published online by Cambridge University Press

where $\boldsymbol{\omega} = \nabla \times \boldsymbol{u} = \omega \boldsymbol{e}_z$ in two-dimensions. The present two-dimensional flow is considered on the orthogonal (x, y) plane, and then the normal unit vector $\boldsymbol{e}_z$ is the z-direction perpendicular to (x, y) plane.

The total hydrodynamic force $\boldsymbol{F}$ is calculated by the integration of the penalization term (e.g. Angot *et al.* 1999; Hejlessen *et al.* 2015) as follows:

$$\boldsymbol{F} = -\rho \int_{\mathcal{D}} \frac{\mathrm{D}\boldsymbol{u}}{\mathrm{D}t}\,\mathrm{d}V = -\rho \int_{\mathcal{D}} \lambda\chi\,(\boldsymbol{u}_S - \boldsymbol{u})\,\mathrm{d}V = -\rho \int_{\mathcal{S}} \lambda(\boldsymbol{u}_S - \boldsymbol{u})\,\mathrm{d}V, \tag{2.4}$$

where the domain $\mathcal{D}$ indicates $\mathcal{D} = \mathcal{S} \cup \mathcal{F}$. The moving velocity $\boldsymbol{u}_S$ of the solid body is obtained as the average velocity inside the domain $\mathcal{S}$, i.e.

$$\boldsymbol{u}_S = \frac{1}{M} \int_{\mathcal{S}} \rho\chi\boldsymbol{u}\,\mathrm{d}V, \tag{2.5}$$

where M is the mass of the solid body. In the present paper, the body is a circular cylinder and it impulsively starts with constant translating velocity without rotation. The flow is two-dimensional and the domain treated in this study is the entire domain, i.e. $\mathcal{S} \sqcup \mathcal{F}$. Furthermore, we use the relative coordinate systems of the fixed with the cylinder, i.e. $\boldsymbol{u}_s = 0$. We also use the condition that the velocity and the vorticity are continuous at the interface between $\mathcal{S}$ and $\mathcal{F}$ in the following analysis.

3. Asymptotic analysis of an initial flow

3.1. *Problem settings*

In this section the asymptotic analysis is carried out for the nonlinear penalized vorticity equation (2.3) with respect to time. As the target situation, the initial flow around an impulsively started circular cylinder is selected. The previous theoretical study of this target flow can be found in Bar-Lev & Yang (1975). They introduced a small parameter $\epsilon = U_o T_o / l_o$ where l_o, T_o and U_o are the reference length, time and velocity, respectively. In their analysis the length l_o is taken as the radius of a cylinder, U_o is the constant moving velocity and T_o is the time. Moreover, the dimensionless time is defined as $t = (U_o/l_o)t^*$ with respect to l_o and U_o. Here, t^* denotes the actual dimensional time.

Figure 1 illustrates the problem setting on the relative coordinate system fixed with the centre of the cylinder. In figure 1 the orthogonal coordinate system (x, y) and the polar coordinate system (r, θ) are taken, and the origin O is set at the centre of the circular cylinder. This study considers the flow past an impulsively started translating circular cylinder at $t = 0$ in a quiescent fluid. In the relative coordinate system, this flow is replaced by the situation that the circular cylinder is abruptly immersed in the uniform flow at $t = 0$, i.e. $U = U_o H(t)$ where $H(t) = 0$ for $t \leqslant 0$ and $H(t) = 1$ for $t > 0$. Therefore, the vorticity can be found to be zero ($\omega = 0$) at $t = 0$.

The target issue is then reduced to a singular perturbation problem with respect to ϵ for the penalized vorticity equation (2.3). We introduce a stretched time T which is defined as $t = \epsilon T$, along the lines of the analysis by Bar-Lev & Yang (1975). Because the penalization parameter λ is taken to be proportional to the inverse of the time step size δt (i.e. $\lambda = \alpha/\delta t$ with the relaxation coefficient α in Hejlesen *et al.* (2015)), we set λ as $\lambda = \lambda_o/\epsilon$ with $\lambda_o = O(1)$. To compare with the analytical results of Bar-Lev & Yang (1975), we assume that the Reynolds number Re is sufficiently large, that is, the kinematic viscosity ν is sufficiently small. Therefore, we can set $\nu = \epsilon\nu_o$ with $\nu_o = O(1)$. The penalized governing

https://doi.org/10.1017/jfm.2021.869 Published online by Cambridge University Press

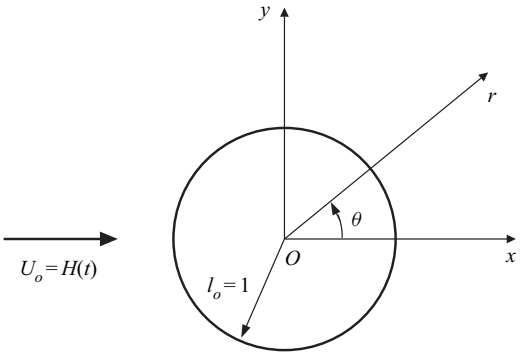


Figure 1. Notations for a circular cylinder abruptly immersed in a constant uniform stream.

equation (2.3) is then written as

$$\frac{\partial \omega}{\partial T} + \epsilon \boldsymbol{u} \cdot \boldsymbol{\nabla} \omega = \epsilon^2 \nu_o \nabla^2 \omega - \lambda_o \boldsymbol{\nabla} \times (\chi \boldsymbol{u}) . \tag{3.1}$$

Note that (3.1) is the dimensionless form with respect to U_o and l_o so that ν_o can be found to be the dimensionless kinematic viscosity. Moreover, this study takes the relative coordinate system fixed with the cylinder, and therefore the velocity of the solid body is $\boldsymbol{u}_S = 0$.

3.2. *Outer solutions*

We first consider the outer solution ω_F^o (denoted by the superscript o) of the governing equation (3.1) in the fluid domain. To do so, ω_F^o is asymptotically expressed as, using the small parameter Δ that is a function of ϵ,

$$\omega_F^o = \omega_{F0}^o + \sum_{n=1}^{\infty} \Delta^n \omega_{Fn}^o. \tag{3.2}$$

The outer solution of the fluid velocity $\boldsymbol{u}_F^o$ is also expressed as

$$\boldsymbol{u}_F^o = \boldsymbol{u}_{F0}^o + \sum_{n=1}^{\infty} \Delta^n \boldsymbol{u}_{Fn}^o. \tag{3.3}$$

Since in the fluid domain $\mathcal{F}$ the characteristic function is $\chi = 0$, (3.1) reduces to $\partial \omega_{F0}^o / \partial T = 0$. Therefore, we can easily find $\omega_{F0}^o = 0$. Similarly, carrying out the recursive calculation in (3.1), we have ω_F^o at the order n as

$$\omega_{Fn}^o = 0, \quad \text{for } n = 0, 1, 2, \ldots . \tag{3.4}$$

Inside the body $\mathcal{S}$ the flow is described by (3.1) set at $\chi = 1$. Since the cylinder is quiescent at $t \leq 0$, the initial vorticity inside the body ω_S^o is zero.

The circular cylinder impulsively immersed in a constant uniform flow at $t = 0$. Noting that $\omega_{F0}^o = 0$ in (3.4), at the early stage of motion, the dominant order of the outer solution in the fluid domain is described by the potential flow solution, i.e.

$$\psi_0^o = \left(r - \frac{1}{r} \right) H(T) \sin\theta, \quad \text{for } r > 1, \tag{3.5}$$

where ψ indicates the stream function whose asymptotic expansion is defined as $\psi = \psi_0^o + \sum_{n=1}^{\infty} \Delta^n \psi_n^0$. Here, the polar coordinates are taken as (r, θ) and they are mainly

https://doi.org/10.1017/jfm.2021.869 Published online by Cambridge University Press

taken in the following sections. Indeed, at the early stage of motion, the higher-order solutions as well as the dominant-order solution of the outer fluid flow are governed by the potential flow (see Bar-Lev & Yang 1975). We can therefore express the stream function at the order n as

$$\psi_n^o = \sum_{m=1} \frac{1}{r^m} \left[A_{mn}^o(T) \sin m\theta + B_{mn}^o(T) \cos m\theta \right], \quad \text{for } r > 1. \tag{3.6}$$

where A_{mn}^o and B_{mn}^o are indeterminate functions of T, respectively. These indeterminate functions can be determined by the matching with the inner solutions (see the following subsection).

3.3. *Inner solutions*

The outer flow of (3.5) causes the slip velocity on the surface of the cylinder (at $r = 1$) so that a non-uniformity domain can be found to exist near the cylinder surface. To remedy this, we stretch the radial coordinate r to R that is defined by $R = (r - 1)/\epsilon$. Then, (3.1) is written as

$$\begin{aligned} \frac{\partial \omega}{\partial T} + u_r \frac{\partial \omega}{\partial R} + \frac{\epsilon}{1 + \epsilon R} u_\theta \frac{\partial \omega}{\partial \theta} = \nu_o \left(\frac{\partial^2}{\partial R^2} + \frac{\epsilon}{1 + \epsilon R} \frac{\partial}{\partial R} + \frac{\epsilon^2}{(1 + \epsilon R)^2} \frac{\partial^2}{\partial \theta^2} \right) \omega \\ - \frac{\lambda_o}{\epsilon} \frac{\partial (\chi u_\theta)}{\partial R} + \frac{\lambda_o \chi}{1 + \epsilon R} \frac{\partial u_r}{\partial \theta} - \frac{\lambda_o \chi}{1 + \epsilon R} u_\theta, \end{aligned} \tag{3.7}$$

where u_r and u_θ are the velocity components of the radial (r) and tangential (θ) directions, respectively. Also, the continuity equation and the vorticity are, respectively, written as

$$\frac{\partial u_r}{\partial R} + \frac{\epsilon}{1 + \epsilon R} \left(u_r + \frac{\partial u_\theta}{\partial \theta} \right) = 0, \quad \omega = \frac{1}{\epsilon} \left[\frac{\partial u_\theta}{\partial R} + \frac{\epsilon}{1 + \epsilon R} \left(u_\theta - \frac{\partial u_r}{\partial \theta} \right) \right]. \tag{3.8a,b}$$

Taking into account (3.8a,b), the velocity components of u_r and u_θ and the vorticity ω are asymptotically expressed as, in the inner domain (denoted by the superscript i),

$$u_r^i = u_{r0}^i + \sum_{n=1} \epsilon^n u_{rn}^i, \quad u_\theta^i = u_{\theta 0}^i + \sum_{n=1} \epsilon^n u_{\theta n}^i, \quad \omega^i = \frac{1}{\epsilon} \left(\omega_0^i + \sum_{n=1} \epsilon^n \omega_n^i \right). \tag{3.9a–c}$$

3.4. *First-order approximation*

Here, the first equation of (3.8a,b) is found to reduce to $\partial u_{r0}^i / \partial R = 0$ for u_{r0}^i. The inner expansion of the first-order outer solution u_{rF}^o needs to be $u_{rF}^{oi} = 2\epsilon R H(T) \cos\theta$ because of (3.5). The matching between u_{Fr}^{oi} and u_{r0}^{io} (i.e. $u_{Fr}^{oi} = u_{r0}^{io}$) then yields

$$u_{r0}^i = 0. \tag{3.10}$$

Note that (3.10) satisfies the matching of the solution inside the body (because of $\boldsymbol{u}_S = 0$). Substituting (3.9a–c) into (3.7) and using (3.10) and the relation of $\omega_0^i = \partial u_{\theta 0}^i / \partial R$ which is obtained from the second equation of (3.8a,b), we can obtain the first-order solution of

https://doi.org/10.1017/jfm.2021.869 Published online by Cambridge University Press

ω^i as, from (3.7),

$$\frac{\partial \omega_0^i}{\partial T} = \nu_o \frac{\partial^2 \omega_0^i}{\partial R^2} - \lambda_o \omega_0^i - \lambda_o \frac{\mathrm{d}\chi}{\mathrm{d}R} u_{\theta 0}^i. \tag{3.11}$$

On the boundary of the cylinder surface, the vorticity is assumed to be continuous as

$$\lim_{R\to 0+} \omega_0^i = \lim_{R\to 0-} \omega_0^i, \tag{3.12}$$

where $R \to 0+$ and $R \to 0-$ means $R \to 0$ from $R > 0$ and from $R < 0$, respectively. From the above relation, we have for $R > 0$ and $R < 0$ that

$$\frac{\partial \omega_0^i}{\partial T} = \nu_o \frac{\partial^2 \omega_0^i}{\partial R^2} - \begin{cases} 0 & \text{for } R > 0, \\ \lambda_o \omega_0^i & \text{for } R < 0. \end{cases} \tag{3.13}$$

The Laplace transform facilitates the analysis of (3.13) because the circular cylinder impulsively starts from rest at $t = 0$. The Laplace transform of ω_0^i is defined as $\Omega_0^i = \mathcal{L}[\omega_0^i] = \int_0^\infty e^{-sT} \omega_0^i(R, \theta; T)\, \mathrm{d}T$ where s is the Laplace complex variable. Then, (3.13) is written as

$$\frac{\partial^2 \Omega_0^i}{\partial R^2} = \frac{1}{\nu_o} \times \begin{cases} s\Omega_0^i & \text{for } R > 0, \\ (s + \lambda_o)\Omega_0^i & \text{for } R < 0. \end{cases} \tag{3.14}$$

As mentioned above, the outer solutions are described by a potential flow inside the fluid domain and $\boldsymbol{u}_S = 0$ inside the cylinder. Taking into account the matching with the outer solutions, we can easily find $\Omega_0^i \to 0$ for $R \to \pm\infty$. Furthermore, the vorticity ω_0^i is continuous at $R = 0$. Therefore, the solution to (3.14) is obtained as

$$\Omega_0^i = \begin{cases} A_0 e^{-\sqrt{s/\nu_o} R} & \text{for } R > 0, \\ A_0 e^{\sqrt{(s+\lambda_o)/\nu_o} R} & \text{for } R < 0, \end{cases} \tag{3.15}$$

where A_0 is an indeterminate function of s and θ. We note that $\partial \omega_0^i / \partial R$ is discontinuous at $R = 0$, i.e. in the present problem there is the slip induced by the radial gradient of the vorticity on the cylinder surface.

Similar to ω_0^i, the Laplace transform of $u_{\theta 0}^i$ is described by $U_{\theta 0}^i = \mathcal{L}[u_{\theta 0}^i]$. Substituting (3.15) into the relation of $\omega_0^i = \partial u_{\theta 0}^i / \partial R$ which is obtained from the second equation of (3.8*a*,*b*), we can obtain

$$U_{\theta 0}^i = \begin{cases} -A_0 \sqrt{\dfrac{\nu_o}{s}} e^{-\sqrt{s/\nu_o} R} + A_1 & \text{for } R > 0, \\ A_0 \sqrt{\dfrac{\nu_o}{s + \lambda_o}} e^{\sqrt{(s+\lambda_o)/\nu} R} + A_1 - \left(\sqrt{\dfrac{\nu_o}{s}} + \sqrt{\dfrac{\nu_o}{s + \lambda_o}} \right) A_0 & \text{for } R < 0, \end{cases} \tag{3.16}$$

where A_1 is an indeterminate function of s and θ. We notice that in the derivation of (3.16) we employed the continuity of $U_{\theta 0}^i$ at $R = 0$, i.e.

$$\lim_{R\to 0+} u_{\theta 0}^i = \lim_{R\to 0-} u_{\theta 0}^i. \tag{3.17}$$

The matching between the outer expansion of (3.16) (i.e. $U_{\theta 0}^{io}$) and the inner expansion of (3.5) (i.e. $\mathcal{L}[u_{\theta 0}^{oi}]$) can determine the indeterminate function A_1 as $A_1 = -(2/s)\sin\theta$. As for the solid domain, the matching with the inner expansion of u_S^o (i.e. $u_S^{oi} = 0$) determines

https://doi.org/10.1017/jfm.2021.869 Published online by Cambridge University Press

the indeterminate function A_1 as $A_1 = A_0\{(\nu_o/s)^{1/2} + [\nu_o/(s+\lambda_o)]^{1/2}]\}$. Therefore, the first approximation of the inner solution for the velocity, $u^i_{\theta 0}$, can be written as

$$u^i_{\theta 0} = \sin\theta \times \begin{cases} u^+_{\theta 0} & \text{for } R > 0, \\ u^-_{\theta 0} & \text{for } R < 0, \end{cases} \tag{3.18}$$

where

$$u^+_{\theta 0} = \mathcal{L}^{-1}\left[-\frac{2}{s} + \frac{2}{\lambda_o}\frac{\sqrt{s+\lambda_o}}{s}\left(\sqrt{s+\lambda_o} - \sqrt{s}\right)e^{-\sqrt{s/\nu_o}R}\right], \tag{3.19}$$

$$u^-_{\theta 0} = -\mathcal{L}^{-1}\left[\frac{2}{\lambda_o}\frac{\sqrt{s+\lambda_o} - \sqrt{s}}{\sqrt{s}}e^{\sqrt{(s+\lambda_o)/\nu_o}R}\right]. \tag{3.20}$$

The inverse Laplace transform of (3.19) and (3.20) are calculated by using the formulae $\mathcal{L}^{-1}[\sqrt{\pi/s}\,e^{-a\sqrt{s}}] = e^{-a^2/(4t)}/\sqrt{t}$ for $a \geqslant 0$, $\mathcal{L}^{-1}[(2\sqrt{\pi}\,e^{-a\sqrt{s}})/a] = e^{-a^2/(4t)}/t^{3/2}$ for $a > 0$, and $\mathcal{L}^{-1}[\sqrt{(s+2a)/s} - 1] = ae^{-at}(I_1(at) + I_0(at))$ where I_n $(n = 0,\ 1)$ is the modified Bessel function of the first kind (see Abramowitz & Stegun (1954), formulae 29.3.84, 29.3.82 and 29.3.48). For $R > 0$, (3.18) becomes, taking the inverse Laplace transform of (3.19) and setting $\eta = R/(2\sqrt{\nu_o T})$,

$$u^i_{\theta 0} = \left\{-2 + 2\,\mathrm{erfc}(\eta) - \frac{\eta}{\sqrt{\pi}}e^{-\lambda_o T/2}\int_0^1 \frac{1}{x^{3/2}}e^{-\eta^2/x + (\lambda_o T/2)x}\right.$$
$$\left.\times\left[I_1\left(\frac{\lambda_o T}{2}(1-x)\right) + I_0\left(\frac{\lambda_o T}{2}(1-x)\right)\right]\mathrm{d}x\right\}\sin\theta. \tag{3.21}$$

Similarly, for $R < 0$, (3.18) becomes

$$u^i_{\theta 0} = \frac{\eta}{\sqrt{\pi}}e^{-\lambda_o T/2}\int_0^1 \frac{1}{x^{3/2}}e^{-\eta^2/x - (\lambda_o T/2)x}$$
$$\times\left[I_1\left(\frac{\lambda_o T}{2}(1-x)\right) + I_0\left(\frac{\lambda_o T}{2}(1-x)\right)\right]\mathrm{d}x\sin\theta. \tag{3.22}$$

The slip velocity on the surface of the cylinder is calculated by setting $R = 0$ in (3.18) giving

$$u^i_{\theta 0} = -\frac{2}{\lambda_o}\mathcal{L}^{-1}\left(\sqrt{\frac{s+\lambda_o}{s}} - 1\right)\sin\theta = -e^{-\lambda_o T/2}\left[I_1\left(\frac{\lambda_o T}{2}\right) + I_0\left(\frac{\lambda_o T}{2}\right)\right]\sin\theta. \tag{3.23}$$

It can be found that the tangential slip velocity at $R = 0$ decreases with $1/\sqrt{\lambda_o}$, i.e. $u^i_{\theta 0} \to O(1/\sqrt{\lambda_o})$ as $\lambda_o \to \infty$. We will later show that the normal slip velocity at $R = 0$ is of the order of $1/\lambda_o$ as $\lambda_o \to \infty$, i.e. $u^i_{r1} \to O(1/\lambda_o)$. This result is the same as the one of Carbou & Fabrie (2003) although the estimation given by Angot *et al.* (1999) is of the order of $1/\lambda_o^{1/4}$. Figure 2 shows the distribution of $u^i_{\theta 0}$ with respect to $\eta = R/(2\sqrt{\nu_o T})$ at $\theta = \pi/2$ (along the y-axis). In the computation of figure 2, the twenty-points Gaussian integration is employed to estimate the integral. Figure 2 compares the first-order solution $u^i_{\theta 0}$ with respect to T at fixed $\lambda_o = 1.0$ (figure 2*a*) and λ_o at fixed $T = 1.0$ (figure 2*b*) against the analytical solution of Bar-Lev & Yang (1975) using the conventional

https://doi.org/10.1017/jfm.2021.869 Published online by Cambridge University Press

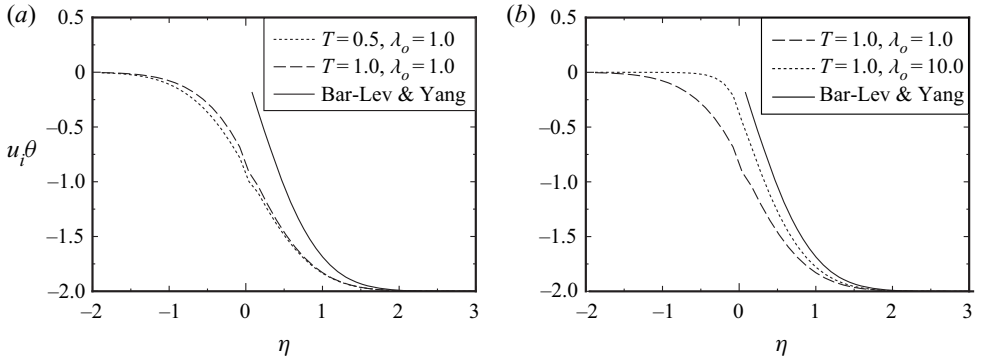


Figure 2. Comparison of the first-order inner solutions of u^i_θ at $\theta = \pi/2$ against the result of Bar-Lev & Yang (1975).

Navier–Stokes equations. As shown in figure 2, the slip velocity arises on the surface of the cylinder, and the strength decreases with increasing λ_o. The strength of the slip velocity is of $O(1/\sqrt{\lambda_o T})$. The velocity distribution of $u^i_{\theta 0}$ is observed to converge to the solution of Bar-Lev & Yang (1975) with increasing λ_o.

Similar to (3.20), the first approximation of the inner solution for the vorticity, ω^i_0, is written as

$$\omega^i_0 = \sin\theta \times \begin{cases} \tilde{\omega}^{i+}_0 & \text{for } R > 0, \\ \tilde{\omega}^{i-}_0 & \text{for } R < 0, \end{cases} \tag{3.24}$$

where

$$\tilde{\omega}^{i+}_0 = -\mathcal{L}^{-1}\left[\frac{2}{\lambda_o\sqrt{\nu_o}}\sqrt{\frac{s+\lambda_o}{s}}\left(\sqrt{s+\lambda_o}-\sqrt{s}\right)e^{-\sqrt{s/\nu_o}R}\right], \tag{3.25}$$

$$\tilde{\omega}^{i-}_0 = -\mathcal{L}^{-1}\left[\frac{2}{\lambda_o\sqrt{\nu_o}}\sqrt{\frac{s+\lambda_o}{s}}\left(\sqrt{s+\lambda_o}-\sqrt{s}\right)e^{\sqrt{(s+\lambda_o)/\nu_o}R}\right]. \tag{3.26}$$

3.5. *Second-order approximation*

Moreover, we proceed to derive the second-order approximation. The first equation of (3.8*a*,*b*) gives the second-order inner solution u^i_{r1} which is written by

$$\frac{\partial u^i_{r1}}{\partial R} = -u^i_{r0} - \frac{\partial u^i_{\theta 0}}{\partial \theta}. \tag{3.27}$$

Substituting (3.10) and (3.18) into (3.27) and taking into account the matching principle with $\boldsymbol{u}_S = 0$ that results in $u^i_{r1} \to 0$ as $R \to -\infty$, we have, using the continuity condition of u_{r1} at $R = 0$,

$$u^i_{r1} = \cos\theta \times \begin{cases} u^+_{r1} & \text{for } R > 0, \\ u^-_{r1} & \text{for } R < 0, \end{cases} \tag{3.28}$$

https://doi.org/10.1017/jfm.2021.869 Published online by Cambridge University Press

where

$$u_{r1}^{+}=2\mathcal{L}^{-1}\left[\frac{\sqrt{\nu_o}}{\lambda_o}\frac{\sqrt{s+\lambda_o}-\sqrt{s}}{s}\left(\sqrt{\frac{s+\lambda_o}{s}}e^{-\sqrt{s/\nu_o}R}-\frac{\lambda_o}{\sqrt{s(s+\lambda_o)}}\right)+\frac{R}{s}\right], \tag{3.29}$$

$$u_{r1}^{-}=2\mathcal{L}^{-1}\left[\frac{\sqrt{\nu_o}}{\lambda_o}\frac{\sqrt{s+\lambda_o}-\sqrt{s}}{\sqrt{s(s+\lambda_o)}}e^{\sqrt{(s+\lambda_o)/\nu_o}R}\right]. \tag{3.30}$$

From the above (3.18), u_{r1} at $R=0$ becomes

$$u_{r1}=2\cos\theta\frac{1}{\lambda_o}\sqrt{\frac{\nu_o}{\pi T}}\left(1-e^{-\lambda_o T}\right). \tag{3.31}$$

The normal slip velocity can be thus found to be of the order of $1/\lambda_o$.

The outer solutions are obtained in (3.5) together with (3.6). The inner expansion of the outer solutions in the fluid domain is therefore written as, differentiating those equations with respect to θ,

$$u_r^{oi}=2\epsilon RH(T)\cos\theta+\Delta\sum_{n=1}n\left(A_{n1}^{o}\cos n\theta-B_{n1}^{o}\sin n\theta\right). \tag{3.32}$$

The outer expansions of the inner solutions (3.18) and (3.28) are obtained for inside and outside the fluid domain. Equating these expansions for the fluid domain we can determine the indeterminate functions:

$$\mathcal{L}[A_{n1}^{o}]=-2\sqrt{\frac{\nu_o}{s(s+\lambda_o)}}\frac{\sqrt{s+\lambda_o}-\sqrt{s}}{s}\delta_{n1},\quad B_{n1}^{o}=0,\quad \Delta=\epsilon. \tag{3.33}$$

For the second-order vorticity ω_1^i, (3.7) reads as

$$\frac{\partial\omega_1^i}{\partial T}+u_{r1}^i\frac{\partial\omega_0^i}{\partial R}+u_{r0}^i\frac{\partial\omega_1^i}{\partial R}+u_{\theta0}^i\frac{\partial\omega_0^i}{\partial\theta}=\nu_o\frac{\partial^2\omega_1^i}{\partial R^2}+\nu_o\frac{\partial\omega_0^i}{\partial R}$$
$$-\lambda_o\frac{\partial}{\partial R}(\chi u_{\theta1}^i)+\lambda_o\chi\frac{\partial u_{r0}^i}{\partial\theta}-\lambda_o\chi u_{\theta0}^i. \tag{3.34}$$

For the second-order vorticity the second equation of (3.8*a*,*b*) reduces to $\partial u_{\theta1}^i/\partial R=\omega_1^i-u_{\theta0}^i$. The Laplace transform of (3.34) gives, taking into account $u_{r0}^i=0$,

$$\frac{\mathrm{d}^2\Omega_1^i}{\mathrm{d}R^2}-\begin{cases}\dfrac{s}{\nu_o}\Omega_1^i=F_+(R,\theta) & \text{for } R>0,\\[2mm] \dfrac{s+\lambda_o}{\nu_o}\Omega_1^i=F_-(R,\theta) & \text{for } R<0.\end{cases} \tag{3.35}$$

Here, the functions $F_\pm(R,\theta)$ are defined for $R>0$ and $R<0$, respectively,

$$F_\pm(R,\theta)=-\mathcal{L}\left[\frac{\partial\omega_0^i}{\partial R}-\frac{u_{r1}^i}{\nu_o}\frac{\partial\omega_0^i}{\partial R}-\frac{u_{\theta0}^i}{\nu_o}\frac{\partial\omega_0^i}{\partial\theta}\right]=F_\pm^s\sin\theta+F_\pm^{cs}\sin\theta\cos\theta, \tag{3.36}$$

in which

$$F_\pm^s=-\mathcal{L}\left[\frac{\partial\tilde{\omega}_0^{i\pm}}{\partial R}\right],\quad F_\pm^{cs}=-\mathcal{L}\left[\frac{u_{r1}^{\pm}}{\nu_o}\frac{\partial\tilde{\omega}_0^{i\pm}}{\partial R}+\frac{u_{\theta0}^{\pm}}{\nu_o}\tilde{\omega}_0^{i\pm}\right]. \tag{3.37a,b}$$

https://doi.org/10.1017/jfm.2021.869 Published online by Cambridge University Press

The ordinary differential equation of (3.36) can be easily solved as, taking into account the matching condition that $\Omega_1^i \to 0$ as $R \to \pm\infty$,

$$\Omega_1 = -\frac{e^{-aR}}{2a}\int_0^R F_+(\xi,\theta)e^{a\xi}\,\mathrm{d}\xi - \frac{e^{aR}}{2a}\int_R^\infty F_+(\xi,\theta)e^{-a\xi}\,\mathrm{d}\xi + D_0 e^{-aR} \quad \text{for } R>0, \tag{3.38}$$

$$\Omega_1 = -\frac{e^{-\hat{a}R}}{2\hat{a}}\int_{-\infty}^R F_-(\xi,\theta)e^{\hat{a}\xi}\,\mathrm{d}\xi - \frac{e^{\hat{a}R}}{2\hat{a}}\int_R^0 F_-(\xi,\theta)e^{-\hat{a}\xi}\,\mathrm{d}\xi + D_1 e^{\hat{a}R} \quad \text{for } R<0, \tag{3.39}$$

where a and $\hat{a}$ are, respectively, defined as

$$a = \sqrt{\frac{s}{\nu_o}}, \quad \hat{a} = \sqrt{\frac{s+\lambda_o}{\nu_o}}. \tag{3.40a,b}$$

In the derivation of (3.38) and (3.39), we used the fact that the integral constants D_0 and D_1 are functions of s and θ. Because the vorticity is continuous at $R=0$, the constants D_0 and D_1 are linked with

$$D_0 - D_1 = \frac{1}{2a}\int_0^\infty F_+(\xi,\theta)e^{-a\xi}\,\mathrm{d}\xi - \frac{1}{2\hat{a}}\int_{-\infty}^0 F_-(\xi,\theta)e^{\hat{a}\xi}\,\mathrm{d}\xi. \tag{3.41}$$

The second-order velocity $u_{\theta 1}^i$ is described by $\partial u_{\theta 1}^i/\partial R = \omega_1^i - u_{\theta 0}^i$ from the second equation of (3.8*a*,*b*) and (3.10). We here define the Laplace transform of $u_{\theta 1}^i$ as $U_{\theta 1}^i = \mathcal{L}[u_{\theta 1}^i]$. Furthermore, we note the matching condition that $U_{\theta 1}^i \to 0$ for $R \to -\infty$. For $R>0$, we then have, using (3.19) and (3.38),

$$\begin{aligned} U_{\theta 1}^i = {} & \frac{1}{2a^2}\left(e^{-aR}\int_0^R F_+(\xi,\theta)e^{a\xi}\,\mathrm{d}\xi - e^{aR}\int_R^\infty F_+(\xi,\theta)e^{-a\xi}\,\mathrm{d}\xi\right) + \frac{1}{a^2}\int_R^\infty F_+(\xi,\theta)\,\mathrm{d}\xi \\ & - \frac{D_0}{a}e^{-aR} + \left[\frac{2}{s}R + \frac{2}{\lambda_o a}\frac{\sqrt{s+\lambda_o}}{s}\left(\sqrt{s+\lambda_o}-\sqrt{s}\right)e^{-aR}\right]\sin\theta + E_0. \end{aligned} \tag{3.42}$$

For $R<0$, we also have, using (3.20) and (3.39),

$$\begin{aligned} U_{\theta 1}^i = {} & \frac{1}{2\hat{a}^2}\left(e^{-\hat{a}R}\int_{-\infty}^R F_- e^{\hat{a}\xi}\,\mathrm{d}\xi - e^{\hat{a}R}\int_R^0 F_- e^{-\hat{a}R}\,\mathrm{d}\xi\right) - \frac{1}{\hat{a}^2}\int_{-\infty}^R F_-\,\mathrm{d}\xi + \frac{D_1}{\hat{a}}e^{\hat{a}R} \\ & + \frac{2}{\lambda_a \hat{a}}\frac{\sqrt{s+\lambda_o}-\sqrt{s}}{\sqrt{s}}e^{\hat{a}R}\sin\theta. \end{aligned} \tag{3.43}$$

The velocity $U_{\theta 1}^i$ is continuous at $R=0$ and, therefore, we have

$$\begin{aligned} E_0 = {} & \frac{D_0}{a} + \frac{D_1}{\hat{a}} + \frac{1}{a^2}\int_0^\infty F_+\left(\frac{e^{-a\xi}}{2}-1\right)\mathrm{d}\xi + \frac{1}{\hat{a}^2}\int_{-\infty}^0 F_-\left(\frac{e^{\hat{a}\xi}}{2}-1\right)\mathrm{d}\xi \\ & + \left[\frac{2}{\lambda_o\hat{a}}\frac{\sqrt{s+\lambda_o}-\sqrt{s}}{\sqrt{s}} - \frac{2}{\lambda_o a}\frac{\sqrt{s+\lambda_o}}{s}\left(\sqrt{s+\lambda_o}-\sqrt{s}\right)\right]\sin\theta. \end{aligned} \tag{3.44}$$

https://doi.org/10.1017/jfm.2021.869 Published online by Cambridge University Press

The matching principle to the outer solution in the fluid domain can determine the function E_0 as, from (3.33),

$$E_0 = \mathcal{L}[A_{11}^o]\sin\theta = -2\sqrt{\frac{\nu_o}{s(s+\lambda_o)}}\frac{\sqrt{s+\lambda_o}-\sqrt{s}}{s}\sin\theta. \tag{3.45}$$

We here consider the asymptotic behaviour of $u_{\theta 1}^i$ for $\lambda_o \gg 1$. Since $F_\pm$ is asymptotically expressed as, taking into account of the order of $u_{\theta 0}^i$ and u_{r1}^i, $F_\pm \sim F_\pm^0 + (1/\sqrt{\lambda_o})F_\pm^1 + O(1/\lambda_o)$. Hence, we have $u_{\theta 1}^i \to O(1/\sqrt{\lambda_o})$. Furthermore, we easily have the following relations at $R = 0$ (i.e. on the cylinder surface), using the physical quantities:

$$u_{\theta 0}^i \sim -\frac{2\sin\theta}{\sqrt{\pi\lambda t}}\left[1 + O(1/(\lambda t))\right], \tag{3.46}$$

$$\frac{\partial u_{\theta 0}^i}{\partial r} \sim -\frac{2\sin\theta}{\sqrt{\pi\nu t}}\left[1 + O(1/(\lambda t))\right]. \tag{3.47}$$

Thus, we can have the following Navier condition on the tangential slip velocity from the first-order solution:

$$u_\theta - \sqrt{\frac{\nu}{\lambda}}\frac{\partial u_\theta}{\partial r} = 0. \tag{3.48}$$

The slip length $\alpha = \sqrt{\nu/\lambda}$ is of the order of $1/\sqrt{\lambda}$ for $\lambda \gg 1$, and of the order of $\sqrt{1/Re}$ for $Re \gg 1$, where Re is the Reynolds number based on the radius of the cylinder and the impulsive constant velocity. This is in qualitatively agreement with the results given by Nguyen van yen *et al.* (2011, 2014).

3.6. *Drag coefficient*

In this subsection, we will derive the drag coefficient from the asymptotic solution which is obtained in the preceding subsections, and verify it against the results of Bar-Lev & Yang (1975). According to Bar-Lev & Yang (1975), the drag coefficient C_D is defined as $C_D = D/[(1/2)\rho U_o^2(2r_o)]$, where U_o is a constant moving velocity and r_o is the radius of a circular cylinder.

As formulated in (2.4), in the penalization method the drag force D is obtained by the integration of the penalization term. Noting that (2.2) and $\boldsymbol{u}_s = 0$ (i.e. $|\boldsymbol{u}_s| \to 0$ as $R \to -\infty$), the drag force D is written as

$$\begin{aligned} D &= \rho\int_V \lambda\chi u_x \,\mathrm{d}V = \rho\lambda_o\int_0^{2\pi}\int_{-1/\epsilon}^0 \left(u_r^i\cos\theta - u_\theta^i\sin\theta\right)(1+\epsilon R)\,\mathrm{d}R\,\mathrm{d}\theta \\ &= \rho\lambda_o\int_0^{2\pi}\text{p.f.}\int_{-\infty}^0 \left(u_r^i\cos\theta - u_\theta^i\sin\theta\right)(1+\epsilon R)\,\mathrm{d}R\,\mathrm{d}\theta, \end{aligned} \tag{3.49}$$

in which the symbol 'p.f.' indicates the Hadamard finite part of integral and u_x is the x component of velocity. Noting that (3.9*a–c*) together with (3.10), (3.49) reduces to

$$\begin{aligned} C_D &= \lambda_o\int_0^{2\pi}\int_{-\infty}^0 \left[-u_{\theta 0}^i\sin\theta + \epsilon\left(u_{r1}^i\cos\theta - u_{\theta 1}^i\sin\theta - Ru_{\theta 0}^i\sin\theta\right)\right]\mathrm{d}R\,\mathrm{d}\theta + O(\epsilon^2) \\ &\approx \lambda_o\pi\int_{-\infty}^0 \left[-u_{\theta 0}^- + \epsilon\left(u_{r1}^- - u_{\theta 1}^{s-} - Ru_{\theta 0}^-\right)\right]\mathrm{d}R. \end{aligned} \tag{3.50}$$

https://doi.org/10.1017/jfm.2021.869 Published online by Cambridge University Press

Here, the function $u^{s-}_{\theta 1}$ indicates the components of $\sin\theta$ involved in $u^{i}_{\theta 1}$, i.e. $u^{i}_{\theta 1} = \mathcal{L}^{-1}[U^{i}_{\theta 1}] = u^{s-}_{\theta 1}\sin\theta + u^{cs-}_{\theta 1}\sin\theta\cos\theta$ for $R < 0$. Substituting the inverse Laplace transform of (3.20), (3.30) and (3.43) into (3.50), the drag coefficient C_D is obtained as (see Appendix A for the detailed derivation)

$$C_D = 2\sqrt{\frac{\nu_o \pi}{T}}\left(1 - e^{-\lambda_o T}\right) + \pi\epsilon\nu_o\left[1 + e^{-\lambda_o T} - 2e^{-\lambda_o T/2} I_0\left(\frac{\lambda_o T}{2}\right)\right]. \tag{3.51}$$

The above, (3.51), becomes as follows, when the physical quantities are replaced by λ, t and ν:

$$C_D = 2\sqrt{\frac{\nu \pi}{t}}\left(1 - e^{-\lambda t}\right) + \pi\nu\left[1 + e^{-\lambda t} - 2e^{-\lambda t/2} I_0\left(\frac{\lambda t}{2}\right)\right]. \tag{3.52}$$

In the analytical result of Bar-Lev & Yang (1975) that is based on the conventional Navier–Stokes equations, the first-order solution of C_D is obtained as $C_D = 4\sqrt{\nu\pi/t}$. In contrast, the present result of (3.51) exhibits $C_D = 2\sqrt{\nu\pi/t}$ as $\lambda \to \infty$. It thus can be found that the first-order solution obtained from the penalization method is a half of the conventional result of Bar-Lev & Yang (1975) as $\lambda \to \infty$.

In the analysis of Bar-Lev & Yang (1975), the drag coefficient is derived from the sum of the friction drag and the pressure drag on the surface of the cylinder, i.e.

$$C_D = \epsilon\nu_o \int_0^{2\pi} \left(\frac{\partial\omega}{\partial r} - \omega\right)_{r=1} \sin\theta \, \mathrm{d}\theta. \tag{3.53}$$

The first term of the integral includes the contribution from the pressure and the second is the contribution from the friction. In their analysis the no-slip condition is imposed on the surface of the cylinder (i.e. $u^{i}_{r} = u^{i}_{\theta} = 0$ at $R = 0$) and, therefore, we have $(1/\rho)(\partial p/\partial\theta) = \nu_o(\partial\omega^{i}/\partial R)$ at $R = 0$. The penalization method does not enforce the no-slip condition on the surface of the cylinder so that such a relation could not fulfilled.

Figure 3 shows a comparison of the pressure coefficient C^{o}_{p} with respect to θ between the present penalization results and the conventional analytical results of Bar-Lev & Yang (1975). In figure 3 the solid lines indicates the present penalization results of $C^{0}_{p} = -4\sin^2\theta - 4\sqrt{\nu_o/(\pi T)}(1 - e^{-\lambda_o T})(1 + \cos\theta) + O(\epsilon^2)$ whereas the dotted lines are the conventional results of Bar-Lev & Yang (1975) of $C^{0}_{p} = -4\sin^2\theta - 4\sqrt{\nu_o/(\pi T)}(1 + \cos\theta) + O(\epsilon^2)$. Here, C^{o}_{p} means the pressure coefficient that is defined by the difference from the front point of the cylinder. It seems that the pressure distributions on the cylinder surface are in nice agreement with the conventional results for $\lambda_o \gg 1$.

Next, we will derive the drag coefficient C_D using (3.53). Omitting the analysis, the final representation of C_D is written as (see Appendix B for the detailed derivation)

$$\begin{aligned} C_D = 4\sqrt{\frac{\pi\nu_o}{T}} - \frac{3}{2\lambda_o}\sqrt{\frac{\pi\nu_o}{T^3}}\left(1 - e^{-\lambda_o T}\right) + \frac{\pi}{4}\frac{\lambda_o}{\epsilon}e^{-\lambda_o T/2}\left[I_0\left(\frac{\lambda_o T}{2}\right) - I_2\left(\frac{\lambda_o T}{2}\right)\right] \\ + \epsilon\nu_o\pi\left\{1 - e^{-\lambda_o T/2}\left[I_1\left(\frac{\lambda_o T}{2}\right) + I_0\left(\frac{\lambda_o T}{2}\right)\right]\right\}. \end{aligned} \tag{3.54}$$

It can be found that (3.54) asymptotically exhibits $C_D \sim 4\sqrt{\nu\pi/t}$ as $\lambda \to \infty$. As shown in Bar-Lev & Yang (1975), the friction drag is the same as the pressure drag for the first order in the case of $\lambda \to \infty$. Hence, since χ is zero in the fluid domain $\mathcal{F}$, there is the possibility that the pressure drag is not taken into account in (3.50) so that (3.51) exhibits

https://doi.org/10.1017/jfm.2021.869 Published online by Cambridge University Press

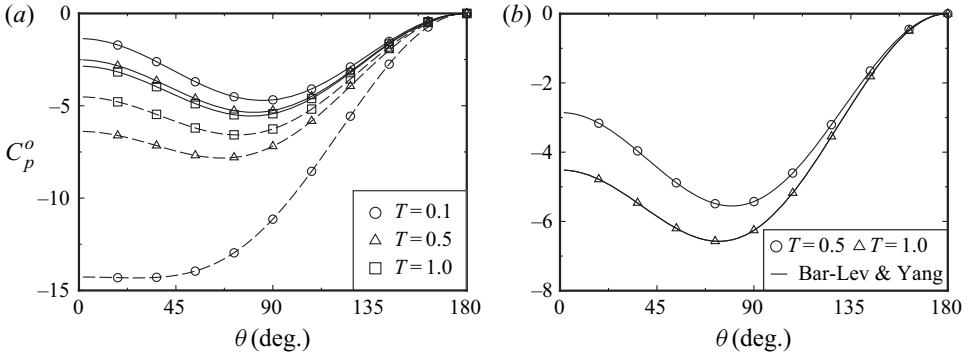


Figure 3. Comparison of the pressure coefficient C_p^o at $\nu_o = 1$ against the conventional result of Bar-Lev & Yang (1975). In panel (*a*), the dashed lines are the results of Bar-Lev & Yang (1975).

the half-value of the results of Bar-Lev & Yang (1975) as $\lambda \to \infty$. This will be a future problem.

Furthermore, we will derive the drag coefficient C_D using the alternative formula that is obtained from the hydrodynamic impulse (see Shiels 1998):

$$C_D = -\frac{\mathrm{d}}{\mathrm{d}t}\int_{\mathcal{F}} y\omega \,\mathrm{d}V = -\frac{\mathrm{d}}{\mathrm{d}T}\int_0^{2\pi} \sin\theta \,\mathrm{d}\theta \int_0^{\infty} \omega^i (1+\epsilon R)^2 \,\mathrm{d}R. \tag{3.55}$$

We here note that T is stretched as $T = t/\epsilon$. Omitting the analysis, the final representation of C_D is written as (see Appendix C for the detailed derivation)

$$C_D = 4\sqrt{\frac{\pi\nu_o}{T}} - \frac{5}{2\lambda_o}\sqrt{\frac{\pi\nu_o}{T^3}}\left(1 - e^{-\lambda_o T}\right) - \frac{\pi}{\epsilon}\frac{\lambda_o}{4}e^{-\lambda_o T/2}\left[I_2\left(\frac{\lambda_o T}{2}\right) - I_0\left(\frac{\lambda_o T}{2}\right)\right]. \tag{3.56}$$

As $\lambda_o \to \infty$, (3.56) behaves like

$$C_D \sim 4\sqrt{\frac{\pi\nu_o}{T}} + \frac{1}{\epsilon}\sqrt{\frac{\pi}{\lambda_o T^3}} - \frac{5}{4\lambda_o}\sqrt{\frac{\pi\nu_o}{T^3}}. \tag{3.57}$$

It can be also found that the present penalization result converges to the same result, i.e. $C_D \sim 4\sqrt{\pi\nu/t}$ of Bar-Lev & Yang (1975) as $\lambda \to \infty$. In (3.55), we note that the integral region is limited to the fluid region. Let us consider the case that the integral region is the inside of the cylinder, i.e. $(\mathrm{d}/\mathrm{d}t)\int_{\mathcal{B}} y\omega \,\mathrm{d}V$. Then, we have (see the detailed derivation in Appendix C)

$$\begin{aligned}\frac{\mathrm{d}}{\mathrm{d}t}\int_{\mathcal{B}} y\omega \,\mathrm{d}V = &-\frac{1}{\lambda_o}\sqrt{\frac{\pi\nu_o}{T^3}}\left(1 - e^{-\lambda_o T}\right) + 2\sqrt{\frac{\nu_o}{\pi T}}e^{-\lambda_o T} + \frac{1}{2}\sqrt{\frac{\pi\nu_o}{T^3}}e^{-\lambda_o T} \\ &+\sqrt{\frac{\pi\nu_o}{T}}\lambda_o e^{-\lambda_o T} + \frac{\pi}{8}\frac{\lambda_o}{\epsilon}e^{-\lambda_o T/2}\left[I_0(\lambda_o T/2) - I_2(\lambda_o T/2)\right].\end{aligned} \tag{3.58}$$

Thus, we can see that the first approximation of C_D is derived from the fluid flow domain $\mathcal{F}$, since from the cylinder flow region $\mathcal{B}$ it is of the order of $1/\sqrt{\lambda}$ as shown in the above equation. These results imply that the flow in the fluid region plays an important role in deriving the drag coefficient.

Figure 4 shows a comparison of C_D at $\nu_o = 1$ between the present penalization result and the conventional result of Bar-Lev & Yang (1975) that is $C_D = 4\sqrt{\pi\nu_o/T} + \pi\epsilon\nu_o(9 -$

https://doi.org/10.1017/jfm.2021.869 Published online by Cambridge University Press

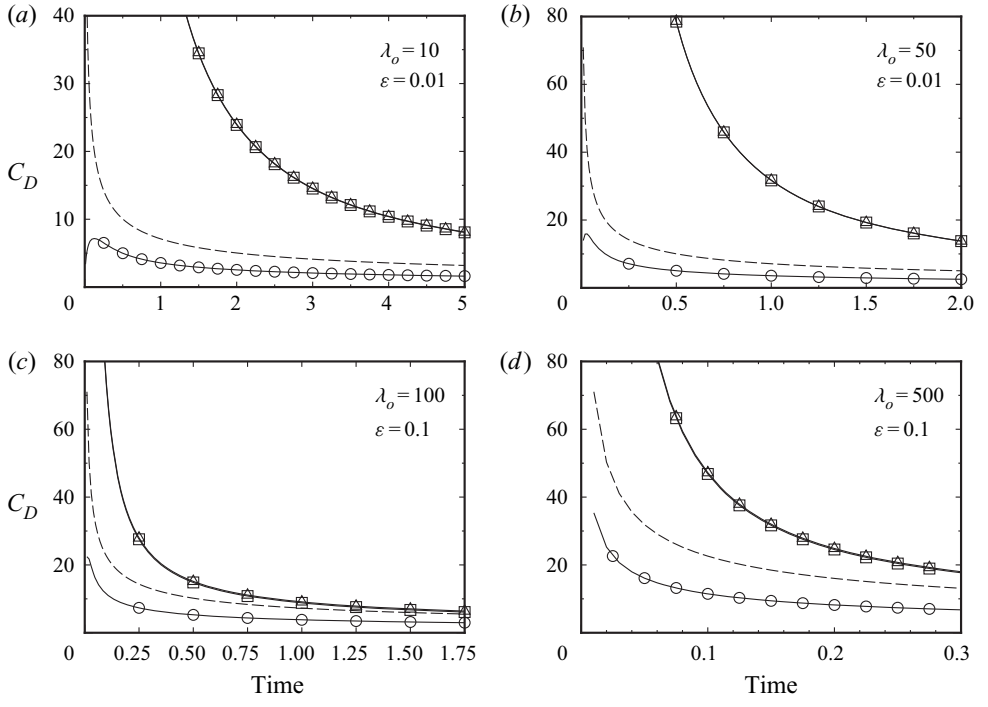


Figure 4. Comparison of the drag coefficient C_D at $v_o = 1$ between several formulae against the conventional result of Bar-Lev & Yang (1975). The symbols used are: circle, (3.51) that is obtained by the integration of the penalization term; triangle, (3.54) that is obtained by the integration of the vorticity and its derivative at $r = 1$; square, (3.56) that is obtained from the hydrodynamic impulse; dashed line, Bar-Lev & Yang (1975).

$15/\sqrt{\pi}$). Figure 4(*a*,*b*) are the results of $\epsilon = 0.01$ and figure 4(*c*,*d*) are of $\epsilon = 0.1$. In figure 4, the result plotted with circles is calculated by (3.51) that is obtained from the integration of the penalization term. The result plotted with triangles is calculated by (3.54) that is obtained from the integration of the vorticity and its derivative at $r = 1$. The results plotted with squares is calculated by (3.56) that is obtained from the hydrodynamic impulse. As observed, two results, except the integration of the penalization term plotted with circles, approach the conventional result of Bar-Lev & Yang (1975) with increasing λ_o. Furthermore, the results of both (3.54) and (3.56) are in nice agreement with each other and, therefore, the fluid flow can be found to be modelled well by the penalization method.

4. Concluding remarks

The asymptotic analysis has been implemented for a Brinkman penalization model of the Navier–Stokes equations. The initial flow past an impulsively started translating circular cylinder is selected for the target problem. The analytical solution of this flow was given by Bar-Lev & Yang (1975) of which solution is called the conventional results of the full Navier–Stokes equations. The present asymptotic solutions for the penalized full Navier–Stokes equations are compared with the conventional analytical solutions.

The significant findings obtained are as follows. In the penalization method the no-slip condition is not enforced on the surface of the cylinder. The present analysis gives the fact that the tangential and normal slip velocities on the cylinder surface with a fixed time are of the order of $1/\sqrt{\lambda}$ and $1/\lambda$ as $\lambda \to \infty$, respectively, which is the same order as the results

https://doi.org/10.1017/jfm.2021.869 Published online by Cambridge University Press

of Carbou & Fabrie (2003). Therefore, it is necessary that the penalization parameter λ is set at a sufficiently large value in the numerical calculation.

Furthermore, this study derived the drag coefficient C_D from the three different formulae: (i) the integration of the penalization term; (ii) the integration of the vorticity and its derivative on the cylinder surface; (iii) the hydrodynamic impulse. As a result, the values of C_D obtained from the formulae (ii) and (iii) are in nice agreement with the conventional result of Bar-Lev & Yang (1975) as $\lambda \to \infty$ but, however, the formula (i) gives a half-value of the result of Bar-Lev & Yang (1975).

Acknowledgments. The authors express their sincere thanks to anonymous referees who kindly introduced many of the references on penalization methods and the relation between the residual slip velocity and the Navier boundary condition.

Funding. This work was supported by JSPS KAKENHI (grant number 21K04757).

Declaration of interests. The authors report no conflict of interest.

Author ORCIDs.
Y. Ueda https://orcid.org/0000-0001-5340-0671.

Appendix A

In this appendix, we obtain the drag coefficient by integrating the penalization term of (3.50). From (3.20), we have

$$\int_{-\infty}^{0} \mathcal{L}[u_{\theta 0}^{-}]\,\mathrm{d}R = -\frac{2}{\lambda_o}\frac{\sqrt{s+\lambda_o}-\sqrt{s}}{\sqrt{s}}\int_{-\infty}^{0} e^{\hat{a}R}\,\mathrm{d}R = -\frac{2\sqrt{\nu_o}}{\lambda_o}\left(\frac{1}{\sqrt{s}}-\frac{1}{\sqrt{s+\lambda_o}}\right). \tag{A1}$$

Therefore, taking the inverse Laplace transform of (A1), we have

$$\int_{-\infty}^{0} u_{\theta 0}^{-}\,\mathrm{d}R = -\frac{2}{\lambda_o}\sqrt{\frac{\nu_o}{\pi T}}\left(1-e^{-\lambda_o T}\right). \tag{A2}$$

Here, $\mathcal{L}[u_{\theta 1}^{s-}]$ is obtained from (3.43) and the function $F_{\pm}^{s}$ is defined by (3.37*a*,*b*). The components of $\sin\theta$ included in D_1 can be obtained as, using (3.41), (3.44) and (3.45),

$$D_1^s = \frac{(\sqrt{s+\lambda_o}-\sqrt{s})^2}{\lambda_o^2}\left(\frac{1}{2}-\frac{\lambda_o}{s}+\frac{1}{2}\sqrt{\frac{s+\lambda_o}{s}}\right). \tag{A3}$$

Using (A3), we have

$$\int_{-\infty}^{0} \mathcal{L}[u_{\theta 1}^{s-}]\,\mathrm{d}R = -\frac{\nu_o}{2\lambda_o}\frac{\sqrt{s+\lambda_o}-\sqrt{s}}{(s+\lambda_o)\sqrt{s}}+\frac{D_1^s}{\hat{a}^2} = \frac{\nu_o}{\lambda_o}\left(\frac{2}{\sqrt{s(s+\lambda_o)}}-\frac{1}{s}-\frac{1}{s+\lambda_o}\right). \tag{A4}$$

The inverse Laplace transform of (A4) gives

$$\int_{-\infty}^{0} u_{\theta 1}^{s-}\,\mathrm{d}R = \frac{\nu_o}{\lambda_o}\left[2e^{-\lambda_o T/2}I_0\left(\frac{\lambda_o T}{2}\right)-1-e^{-\lambda_o T}\right]. \tag{A5}$$

From (3.10) and (3.27), we have $\partial u_{r1}^{-}/\partial R = -u_{\theta 0}^{-}$ and we then perform the integration by parts,

$$\int_{-\infty}^{0} u_{r1}^{-}\,\mathrm{d}R = -\int_{-\infty}^{0} R\frac{\partial u_{r1}^{-}}{\partial R}\,\mathrm{d}R = \int_{-\infty}^{0} R u_{\theta 0}^{-}\,\mathrm{d}R. \tag{A6}$$

https://doi.org/10.1017/jfm.2021.869 Published online by Cambridge University Press

Therefore, we have

$$C_D = -\pi\lambda_o \int_{-\infty}^{0} u_{\theta 0}^{-}\,\mathrm{d}R - \epsilon\pi\lambda_o \int_{-\infty}^{0} u_{\theta 1}^{s-}\,\mathrm{d}R$$
$$= 2\sqrt{\frac{\pi\nu_o}{T}}\left(1 - e^{-\lambda_o T}\right) + \epsilon\pi\nu_o\left[1 + e^{-\lambda_o T} - 2e^{-\lambda_o T/2} I_0\left(\frac{\lambda_o T}{2}\right)\right]. \tag{A7}$$

Appendix B

To obtain the drag coefficient C_D, we select the function $G = (1/\epsilon)\partial_R\Omega_0 - \Omega_0 + \epsilon[\Omega_1 - (1/\epsilon)\partial_R\Omega_1]$ at $R = 0$. Indeed, the components of $\sin\theta$ included in G affect the derivation of C_D and, therefore, we define the $\sin\theta$ components of G as G^s. The first-term of G^s at $R = 0$ is given by (3.24) and (3.25) as

$$\text{(first term of } G^s) = \frac{2}{\epsilon^2\nu_o}\left[1 + \frac{s}{\lambda_o}\left(1 - \frac{\sqrt{s+\lambda_o}}{\sqrt{s}}\right)\right]$$
$$+ \frac{2}{\epsilon\lambda_o\sqrt{\nu_o}}\left(\sqrt{s} + \frac{\lambda_o}{\sqrt{s}} - \frac{s+\lambda_o}{\sqrt{s+\lambda_o}}\right). \tag{B1}$$

From (3.38), the second-term of G^s at $R = 0$ is given by

$$\text{(second term of } G^s) = \frac{1}{2\epsilon}\int_0^\infty F_+^s e^{-a\xi}\,\mathrm{d}\xi + \frac{a}{\epsilon}D_0^s - \frac{1}{2a}\int_0^\infty F_+^s e^{-a\xi}\,\mathrm{d}\xi + D_0^s, \tag{B2}$$

where D_0^s is the $\sin\theta$ components of D_0 which are obtained from (3.41), (3.44) and (3.45), i.e.

$$D_0^s = \frac{1}{\lambda_o^2}\left(1 - \frac{3}{2}\frac{s+\lambda_o}{s} - \frac{1}{2}\sqrt{\frac{s+\lambda_o}{s}}\right) = \frac{5}{2\lambda_o}\left(\sqrt{\frac{s+\lambda_o}{s}} - 1\right) - \frac{3}{2}\frac{1}{s}. \tag{B3}$$

Equation (B3) is obtained by integrating $F_\pm^s$ that is given in (3.37*a*,*b*). Similarly, using (3.37*a*,*b*) the second term of G^s can be obtained. Therefore, we can finally arrive at (3.54).

Appendix C

In this appendix, we will obtain the drag coefficient from (3.55). To do this, we consider the following integral:

$$A = \int_0^{2\pi} \sin\theta\,\mathrm{d}\theta \int_0^\infty \mathcal{L}[\omega^i](1 + \epsilon R)^2\,\mathrm{d}R. \tag{C1}$$

Then, the drag coefficient is written as $C_D = -(\mathrm{d}/\mathrm{d}T)(\mathcal{L}^{-1}[A])$. Also, $\mathcal{L}[\omega^i]$ is expanded as $(1/\epsilon)(\Omega_0 + \epsilon\Omega_1 + \cdots)$. Since Ω_0 is given in (3.24) and (3.25), we have

$$\int_0^\infty \Omega_0\,\mathrm{d}R = -\frac{2}{\lambda_o}\frac{\sqrt{s+\lambda_o}}{s}\left(\sqrt{s+\lambda_o} - \sqrt{s}\right)\sin\theta, \tag{C2}$$

$$\int_0^\infty R\Omega_0\,\mathrm{d}R = -\frac{2\sqrt{\nu_o}}{\lambda_o}\frac{\sqrt{s+\lambda_o}}{s\sqrt{s}}\left(\sqrt{s+\lambda_o} - \sqrt{s}\right)\sin\theta. \tag{C3}$$

https://doi.org/10.1017/jfm.2021.869 Published online by Cambridge University Press

Using (3.38), we have also that

$$\int_0^\infty \Omega_1 \,\mathrm{d}R = \frac{1}{2a^2}\int_0^\infty F_+ e^{-a\xi}\,\mathrm{d}\xi - \frac{1}{a^2}\int_0^\infty F_+\,\mathrm{d}\xi + \frac{D_0}{a}. \tag{C4}$$

Therefore, we have

$$\mathcal{L}^{-1}[A] = \frac{\pi}{\epsilon}\left[-2H(T) + e^{-\lambda_o T/2}\left(I_1\left(\frac{\lambda_o T}{2}\right) + I_0\left(\frac{\lambda_o T}{2}\right)\right)\right]$$
$$+\pi\left[-8\sqrt{\frac{\nu_o T}{\pi}} - \frac{5}{\lambda_o}\sqrt{\frac{\nu_o}{\pi T}}(1 - e^{-\lambda_o T/2}) + 10\sqrt{\frac{\nu_o}{\pi\lambda_o}}\,\mathrm{Erf}\left(\sqrt{\lambda_o T}\right) + O(\epsilon^2)\right]. \tag{C5}$$

Let us consider the case that the integral region is inside the cylinder, i.e.

$$B = \int_0^{2\pi}\sin\theta\,\mathrm{d}\theta\int_{-\infty}^0 \mathcal{L}[\omega^i](1+\epsilon R)^2\,\mathrm{d}R. \tag{C6}$$

Here, we use the relations of

$$\int_{-\infty}^0 \Omega_0^-\,\mathrm{d}R = \int_{-\infty}^0 \frac{\partial U_0^-}{\partial R}\,\mathrm{d}R = -\frac{2}{\lambda_o}\frac{\sqrt{s+\lambda_o}-\sqrt{s}}{\sqrt{s}}\sin\theta, \tag{C7}$$

$$\int_{-\infty}^0 R\Omega_0^-\,\mathrm{d}R = -\int_{-\infty}^0 U_0^-\,\mathrm{d}R = \frac{2}{\lambda_o}\frac{\sqrt{s+\lambda_o}-\sqrt{s}}{\sqrt{s}}\sqrt{\frac{\nu_o}{s+\lambda_o}}\sin\theta. \tag{C8}$$

Furthermore, we use

$$\int_0^{2\pi}\sin\theta\,\mathrm{d}\theta\int_{-\infty}^0 \Omega_1^-\,\mathrm{d}R$$
$$= \pi\int_{-\infty}^0\left[D_1^s e^{\hat{a}R} - \frac{e^{\hat{a}R}}{2\hat{a}}\int_{-\infty}^R F_-^s e^{\hat{a}\xi}\,\mathrm{d}\xi - \frac{e^{-\hat{a}R}}{2\hat{a}}\int_R^0 F_-^s e^{-\hat{a}\xi}\,\mathrm{d}\xi\right]\mathrm{d}R, \tag{C9}$$

where D_1^S is the $\sin\theta$ component of D_1. Thus, we have

$$\int_0^{2\pi}\sin\theta\,\mathrm{d}\theta\int_{-\infty}^0 \Omega_1^-\,\mathrm{d}R = -\pi\left[\frac{5}{2}\frac{\sqrt{\nu_o}}{\lambda_o}\left(\frac{1}{\sqrt{s+\lambda_o}} - \frac{1}{\sqrt{s}}\right) + \sqrt{\frac{\nu_o}{s+\lambda_o}}\right.$$
$$\left. -\frac{1}{2}\sqrt{\frac{\nu_o}{s(s+\lambda_o)}}(\sqrt{s+\lambda_o}-\sqrt{s})\right]. \tag{C10}$$

Therefore, we can finally arrive at

$$\mathcal{L}^{-1}[B] = -\frac{\pi}{\epsilon}e^{-\lambda_o T/2}\left[I_0(\lambda_o T/2) + I_1(\lambda_o T/2)\right] + \frac{2\pi}{\lambda_o}\sqrt{\frac{\nu_o}{\pi T}}\left(1 - e^{-\lambda_o T}\right)$$
$$-\pi\sqrt{\frac{\nu_o}{\pi T}}e^{-\lambda_o T}. \tag{C11}$$

https://doi.org/10.1017/jfm.2021.869 Published online by Cambridge University Press

References

Abramowitz, M.A. & Stegun, A. 1954 *Handbook of Mathematical Functions with Formulas, Graphs, and Mathematical Tables*. Dover.

Al-Mdallal, Q.M. 2012 A numerical study of initial flow past a circular cylinder with combined streamwise and transverse oscillation. *Comput. Fluids* **63**, 174–183.

Angot, P. 2011 On the well-posed coupling between free fluid and porous viscous flows. *Appl. Maths Lett.* **24**, 803–810.

Angot, P., Bruneau, C.-H. & Fabrie, P. 1999 A penalization method to take into account obstacles in incompressible viscous flows. *Numer. Math.* **81**, 497–520.

Badr, H.M. & Dennis, S.C.R. 1985 Time-dependent viscous flow past an impulsively started rotating and translating circular cylinder. *J. Fluid Mech.* **158**, 447–488.

Bar-Lev, M. & Yang, H.T. 1975 Initial flow field over an impulsively started circular cylinder. *J. Fluid Mech.* **72**, 625–647.

Bost, C., Cottet, G.-H. & Maitre, E. 2010 Convergence analysis of a penalization method for the three-dimensional motion of a rigid body in an incompressible viscous fluid. *SIAM J. Numer. Anal.* **48**, 1313–1337.

Carbou, G. 2004 Penalization method for viscous incompressible flow around a porous thin layer. *Nonlinear Anal.* **5**, 815–855.

Carbou, G. 2008 Brinkmann model and double penalization method for the flow around a porous thin layer. *J. Math. Fluid Mech.* **10**, 126–158.

Carbou, G. & Fabrie, P. 2003 Boundary layer for a penalization method for viscous incompressible flow. *Adv. Diff. Equ.* **8** (12), 1453–1480.

Collins, W.M. & Dennis, S.C.R. 1973 The initial flow past an impulsively started circular cylinder. *Q. J. Mech. Appl. Maths* **26** (1), 53–75.

Engels, T., Kolomenskiy, D., Schneider, K. & Sesterhenn, J. 2015 Numerical simulation of fluid-structure interaction with volume penalization method. *J. Comput. Phys.* **281**, 96–115.

Feireisl, E., Neustupa, J. & Stebel, J. 2010 Convergence of a Brinkman-type penalization for compressible fluid flow. *Mathematical Institute of Academy of Science of the Czech Republic*, Preprint No. 2010-013.

Gazzola, M., Chatelain, P., van Rees, W.M. & Koumoutsakos, P. 2011 Simulations of single and multiple swimmers with non-divergence free deforming geometries. *J. Comput. Phys.* **230**, 7093–7114.

Hejlesen, M.M., Koumoutsakos, P., Leonard, A. & Walther, J.H. 2015 Iterative Brinkman penalization for remeshed vortex methods. *J. Comput. Phys.* **280**, 547–562.

Kadoch, B., Kolomenskiy, D., Angot, P. & Schneider, K. 2012 A volume penalization method for incompressible flows and scalar advection-diffusion with moving obstacles. *J. Comput. Phys.* **231**, 4365–4383.

Kevlahan, N.K.-R. & Vasilyev, O. 2005 An adaptive wavelet collocation method for fluid-structure interaction at high Reynolds numbers. *SIAM J. Sci. Comput.* **26** (6), 1894–1915.

Kolomenskiy, D. & Schneider, K. 2009 A Fourier spectral method for the Navier–Stokes equations with volume penalization for moving solid obstacles. *J. Comput. Phys.* **228**, 5687–5709.

Koumoutsakos, P. & Leonard, A. 1995 High-resolution simulations of the flow around an impulsively started cylinder using vortex methods. *J. Fluid Mech.* **296**, 1–38.

Koumoutsakos, P., Leonard, A. & Pépin, F. 1994 Boundary conditions for viscous vortex methods. *J. Comput. Phys.* **113**, 52–61.

Mimeau, C., Cottet, G.-H. & Mortazavi, I. 2015 Vortex penalization method for bluff body flows. *Intl J. Numer. Meth. Fluids* **79**, 55–83.

Mittal, H.V.R., Ray, R.K. & Al-Mdallal, Q.M. 2017 A numerical study of initial flow past an impulsively started rotationally oscilating circular cylinder using a transformation-free HOC scheme. *Phys. Fluids* **29** (9), 093603.

Nguyen van yen, R., Farge, M. & Schneider, K. 2011 Energy dissipating structures produced by walls in two-dimensional flows at vanishing viscosity. *Phys. Rev. Lett.* **106**, 184502.

Nguyen van yen, R., Kolomenskiy, D. & Schneider, K. 2014 Approximation of the Laplace and Stokes operators with Dirichlet boundary conditions through volume penalization; a spectral viewpoint. *Numer. Math.* **128**, 301–338.

Rasmussen, J.T., Cottet, G.-H. & Walther, J.H. 2011 A multiresolution remeshed Vortex-In-Cell algorithm using patches. *J. Comput. Phys.* **230**, 6742–6755.

Rossinelli, D., Bergdorf, M., Cottet, G.-H. & Koumoutsakos, P. 2010 GPU accelerated simulations of bluff body flows using vortex particle methods. *J. Comput. Phys.* **229**, 3316–3333.

https://doi.org/10.1017/jfm.2021.869 Published online by Cambridge University Press

SCHNEIDER, K. & FARGE, M. 2002 Adaptive wavelet simulation of a flow around an impulsively started cylinder using penalization. *Appl. Comput. Harmon. Anal.* **12**, 374–380.

SCHNEIDER, K. & FARGE, M. 2005 Numerical simulation of the transient flow behavior in tube bundles using a volume penalization method. *J. Fluids Struct.* **20**, 555–566.

SCHNEIDER, K., PAGET-GOY, M., VERGA, A. & FARGE, M. 2014 Numerical simulation of flows past flat plates using volume penalization. *Comput. Appl. Maths* **33**, 481–495.

SHIELS, D. 1998 Simulation of controlled bluff body flow with a viscous vortex method. Ph.D. dissertation, Caltech.

UCHIYAMA, T., GU, Q., DEGAWA, T., IIO, S., IKEDA, T. & TAMURA, K. 2020 Numerical simulations of the flow and performance of a hydraulic Savonius turbine by the vortex in cell with volume penalization. *Renewable Energy* **157**, 482–490.

VERMA, S., ABBATI, G., NOVATI, G. & KOUMOUTSAKOS, P. 2017 Computing the force distribution on the surface of complex, deforming geometries using vortex method and Brinkman penalization. *Intl J. Numer. Meth. Fluids* **85**, 484–501.

https://doi.org/10.1017/jfm.2021.869 Published online by Cambridge University Press